Landes Bioscience www.landesbioscience.com

Supplemental Material to:

Myungjin Kim, Hae Li Park, Hwan-Woo Park,
Seung-Hyun Ro, Samuel G. Nam, John M. Reed,
Jun-Lin Guan and Jun Hee Lee

Drosophila Fip200 is an essential regulator of autophagy that attenuates both growth and aging

Autophagy 2013; 9(8)
http://dx.doi.org/10.4161/auto.24811

www.landesbioscience.com/journals/autophagy/article/24811

Kim_FigS1

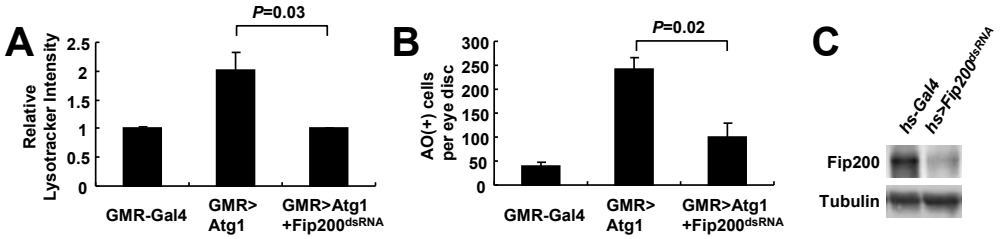

Kim_FigS2

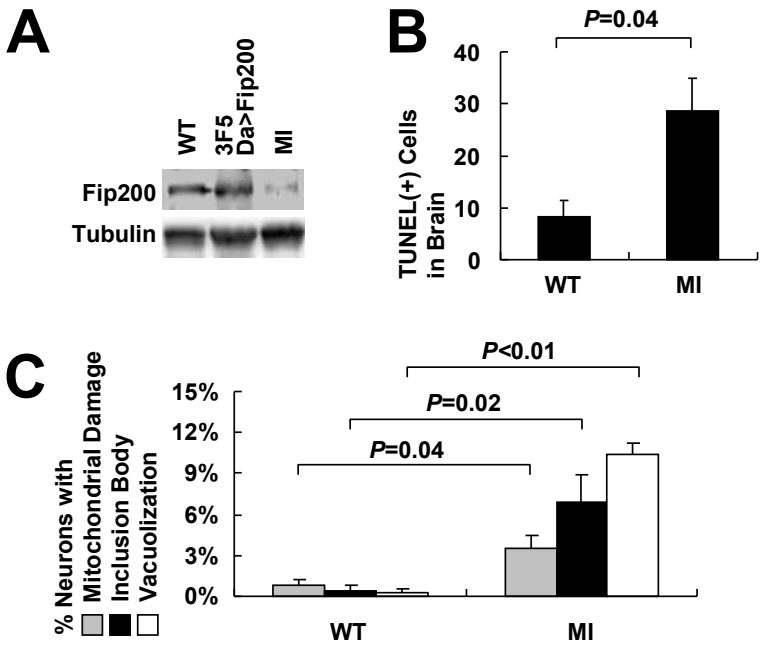

Kim_FigS3

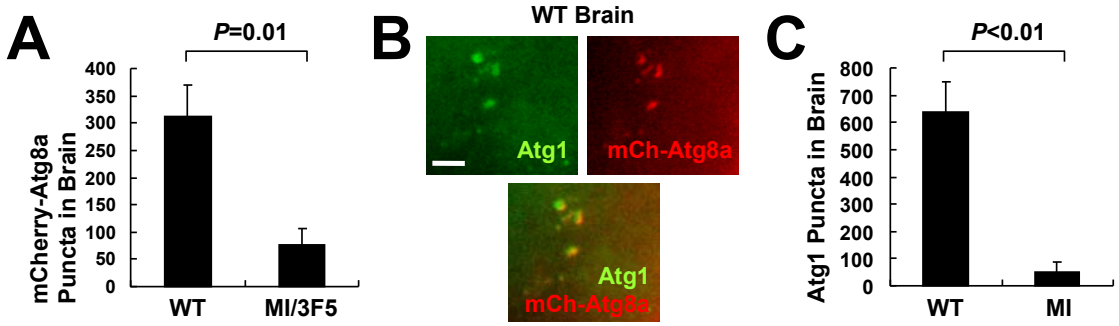

Kim_FigS4

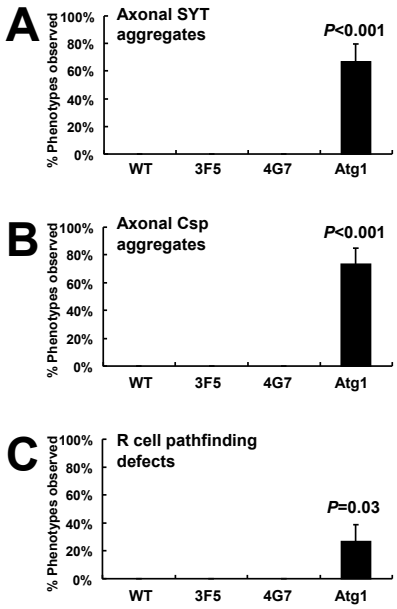

Kim_FigS5

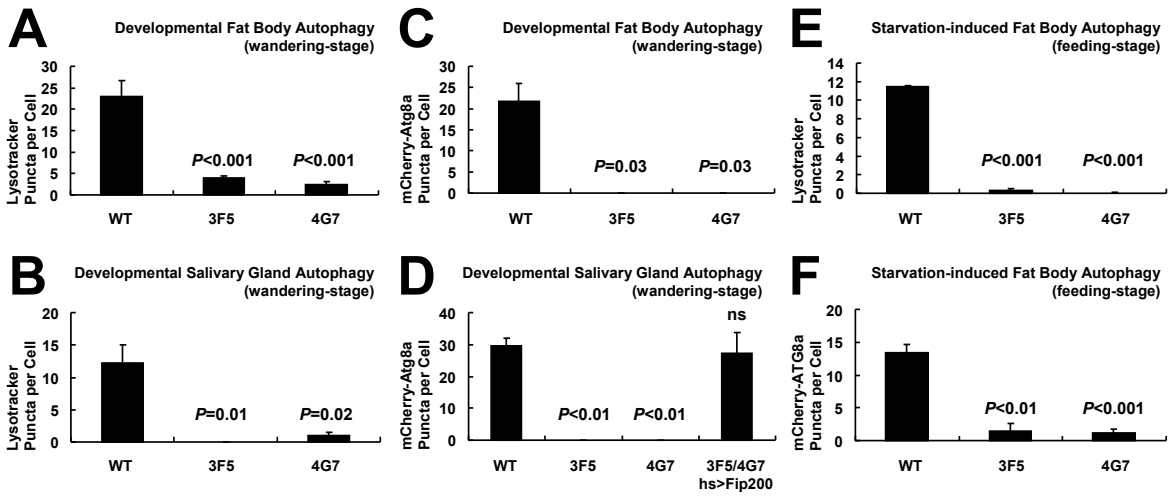

Kim_FigS6

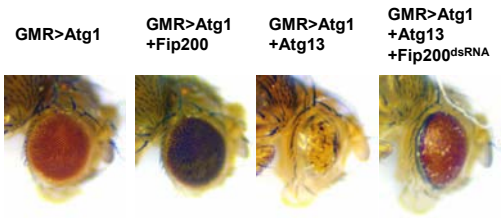

Kim_FigS7

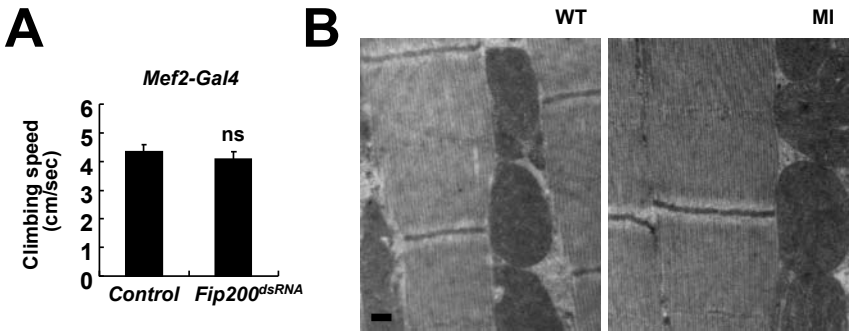

Kim_TableS1

Allele	Nature	Phenotype	Full genotype
WT	Wild-type	Phenotypically normal (N)	w^{1118} control
MI	Minos insertion (Hypomorph) at *FIP200* locus	Wing Posture defective (WP)	$Fip200^{MI01469}$
RV	Revertant of MI	Phenotypically normal (N)	$Fip200^{MI01469\text{-}RV}$
EY	P-element insertion at *Fip200* locus	Phenotypically normal (N)	$Fip200^{EY03045}$
3F5	Null mutant of *Fip200*	Death at pharate adult stage (D)	$Fip200^{3F5}$
4G7	Null mutant of *Fip200*	Death at pharate adult stage (D)	$Fip200^{4G7}$
DF	Deficiency containing *FIP200* locus	Embronic/early larval lethal (E)	$Fip200^{Df(3R)Exel7283}$
Atg1	Transheterozygotic null mutant of *Atg1*	Pupal lethal (P)	$Atg1^{\Delta 3d}/Atg1^{Df(3)BSC10}$

Kim_TableS2

	WT	MI	3F5	4G7	DF	RV	EY
WT	N	N	N	N	N	N	N
MI		WP	WP	WP	WP	N	N
3F5			D	D	D	N	N
4G7				D	D	N	N
DF					E	N	N
RV						N	N
EY							N

Kim_TableS3

	MI	MI/4G7	MI/3F5	MI/RV
WT	2.3E-12	4.1E-10	1.8E-15	1.0
MI		0.6	0.9	3.3E-07
MI/4G7			0.5	1.0E-06
MI/3F5				9.0E-10

Figure S1. dsRNA-mediated silencing of Fip200 inhibits Atg1-induced autophagic cell death, related to Fig. 1. (**A**) Relative LysoTracker Red intensity of GMR-positive regions (posterior to the morphogenetic furrow) of the indicated eye discs shown in Fig. 1K, normalized by the intensity of each GMR-negative regions (anterior to the morphogenetic furrow, n=3). (**B**) Number of apoptotic cells in GMR-positive regions of the indicated eye disc shown in Fig. 1L (n=3). (**C**) 3-day-old adult flies expressing *hs-Gal4* or *hs>Fip200*^{dsRNA} were reared at 29°C for 1 week and then analyzed by immunoblotting using the indicated antibodies. Quantification data are represented as means ± standard error. *P* values were calculated using Student's t-test. Approximate molecular weights (observed/predicted): Fip200 (150 to 200/152kD), Tubulin (50/52kD).

Figure S2. Loss of Fip200 provokes neurodegeneration, related to Fig. 2. (**A**) 3-day-old adult files of w^{1118} (WT), *UAS-Fip200*/+; *Fip200*^{3F5}/*da-Gal4 Fip200*^{3F5} (3F5 Da>Fip200) and *Fip200*^{MI} (MI) strains were analyzed by immunoblotting using the indicated antibodies. (**B**) Number of apoptotic cells in central brain region shown in Fig. 2K (n≥3). (**C**) Percentage of neuronal cells exhibiting the indicated degenerative morphology determined from the transmission electron micrograph images shown in Fig. 2L (n≥3). Quantification data are represented as means ± standard error. *P* values were calculated using Student's t-test. Approximate molecular weights (observed/predicted): Fip200 (150 to 200/152kD), Tubulin (50/52kD).

Figure S3. Autophagy defects in Fip200-deficient brain, related to Fig. 3. (**A**) Number of mCherry-Atg8a puncta in central brain region of the indicated flies shown in Fig. 3G and 3H (n≥3). (**B**) Colocalization of mCherry-Atg8a (red) and Atg1 (green) in *hs>mCherry-Atg8a*/+ (WT) brain. (**C**) Number of Atg1-positive puncta in central brain region of the indicated flies shown in Fig. 3I and 3J (n≥3). Scale bar: 10 μm. Quantification data are represented as means ± standard error. *P* values were calculated using Student's t-test.

Figure S4. Axonal transport and projection are unaffected by Fip200 loss, related to Fig. 4. (**A-C**) Observed frequencies of axonal transport and projection defects, monitored by synaptotagmin aggregation (**A**, related to Fig. 4A), Csp aggregation (**B**, related to Fig. 4B) and photoreceptor pathfinding defects (**C**, related to Fig. 4C) from the indicated fly strains. Quantification data are represented as means ± standard error (n=15). *P* values were calculated between WT and indicated groups, using Student's t-test.

Figure S5. Developmental and starvation-induced autophagy is abrogated by Fip200 loss, related to Fig. 5. (**A-F**) Number of LysoTracker Red or mCherry-Atg8a puncta per cell in salivary glands or fat bodies (n≥60). Flies of the indicated genotypes were staged and treated as described. Quantification data are represented as means ± standard error. *P* values were calculated between WT and indicated groups, using Student's t-test. ns: not significant ($P \geq 0.05$).

Figure S6. Genetic interaction among Atg1, Atg13 and Fip200 in Drosophila eyes. Photographs of adult eye from the indicated fly strains are shown.

Figure S7. Muscle structure and function are unaffected by Fip200 loss. (**A**) 2-week-old *Mef2-Gal4* (Control) and *Mef2>Fip200*^{dsRNA} flies were assayed for climbing abilities. Quantification data are represented as means ± standard error (n≥20). *P* value was calculated between control and indicated groups, using Student's t-test. ns: not significant (*P*≥0.05). (**B**) Transmission electron micrograph of indirect flight muscle from 2-week-old flies of the indicated genotypes. Scale bar: 10 μm.

Table S1. List of *Fip200* and *Atg1* alleles and their phenotypes. For detailed description about the nature of each strain, please see Materials and Methods in the main text.

Table S2. Complementation test between *Fip200* alleles. Phenotypes of flies with the indicated allelic combination are described: N, phenotypically normal; WP, wing posture defective; D, death at pharate adult stage; E, embryonic or early larval lethal.

Table S3. Statistical comparison of the climbing speed between fly strains. The climbing speed was analyzed as in Fig. 2F. *P* values were calculated between the indicated groups of flies using Student's t-test and are indicated in the table. Grey-shaded cells indicate the absence of statistical significance.